Int. J. Nanoelectronics and Materials **5** (2012) 133-148

Electron transport analysis in quantum well HEMT with hot electron mobility model

Sanjoy Deb[1], N Basanta Singh[2], A K De[3], Subir Kumar Sarkar [1,*]

[1]*Department of Electronics & Telecommunication Engineering, Jadavpur University, Kolkata-700032, India*
[2]*Department of Electronics & Communication Engineering, Manipur Institute of Technology, Imphal -795004, India*
[3]*Department of Electronics & Communication Engineering, National Institute of Technology, Durgapur -713201, India*

Received 2 Feb. 2011; Revised 23 Feb. 2011; Accepted 28 March 2011

Abstract

A hot electron analytical model of quantum well high electron mobility transistor is proposed. Our model takes into account the dependence of mobility on different scattering mechanisms. The carrier scattering by polar optic phonons, acoustic deformation potential and background ionized impurities are incorporated in the calculation of mobility considering the carrier distribution to be heated drifted Fermi-Dirac distribution. The proposed model is used to determine the drain current and transconductane of a $Al_xGa_{1-x}As/GaAs$ quantum well high electron mobility transistor. The results obtained using our model is found to agree with experimental results thereby establishing the validity of the proposed model.

Keywords Quantum well; Carrier scattering; Carrier mobility.
PACS: 85.30.De; 73.21.Fg; 72.80.Ey.

1. Introduction

Considerable progress has been made since the first high electron mobility transistor ($Al_xGa_{1-x}As/GaAs$ HEMT) was introduced in the year 1980 [1] and many theoretical and experimental research have been carried out to explain the operation of HEMT's. A model for channel charge and current, as a function of gate and drain voltage, was first developed by Delagebeaudeuf and Linh [2]. Lee et al extended this model to include the variation of Fermi energy of the two-dimensional electron gas with density by using a linearized version of this variation [3-6]. Despite all the experimental and theoretical breakthroughs, research in HEMT continues to be of significant interest of researchers [7-8].

Since its invention, many analytical models of HEMT structure have been proposed and developed using the drift-diffusion model which efficiently described the functionality of such devices. Transport parameters, mobility (μ_n), Einstein coefficient (D_n) etc. used in these models are taken from experimental measurement results [9]. However, the situation is much more complex for advanced HEMT structure. In a short channel HEMT structure, μ_n and D_n are no longer material and field dependent parameters; they depend on microscopic physics, on the structure of the device and even on the applied bias. Under these circumstances, deep

*) For correspondence, E-mail: su_sircir@yahoo.co.in

understanding of electron transport is essential for the device engineers since different transport parameters should be computed from first principles [10].

As stated above electron mobility is one of the most important parameter for analytical modeling of HEMT structure and it depends on material parameters, structural parameters, operational parameters as well as different physical phenomena [10]. With further down-scaling of devices, some unavoidable physical phenomena will considerably modify device performance [11]. Incorporation of these physical phenomena in analytical mobility model is the major issue with current HEMT analytical modeling. Hot electron effect, sheet concentration variation, inter-sub-band scattering, velocity over-shoot, ballistic transport etc have very strong influence on the performance of short channel HEMT. Some issues related to the short channel HEMT structure are as follows;

1. Due to high field in a short channel device, electron temperature is significantly different from lattice temperature thereby establishing the hot electron condition [11]. Under hot electron condition, normal Fermi-Dirac distribution function is inadequate to predict electron distribution in a particular sub-band.
2. 2-D carrier concentration or sheet concentration is a function of both the gate and channel potential. Since the potential along the channel is not constant, there is variation of sheet concentration along the channel.
3. Velocity overshoot occurs whenever there is a difference in the energy and momentum relaxation times and the electron distribution is heated rapidly to energies much greater than the steady-state average energy, especially at the drain end [12].
4. At low field, electrons in quantum well (QW) occupy the lowest sub-band. If the applied field is sufficiently high, electrons gain sufficient energy and are transferred to higher sub-bands via phonon or other scattering mechanisms; initiation of inter-sub-band scattering.
5. Ballistic transport occurs when transport of carriers occur without any collision and this happens when device dimensions are equal to or smaller than the scattering mean free path for electrons [13].

Analytical mobility model should consider the above issues carefully for accurate modeling of short channel HEMT structure. Many mobility models of HEMT have already been proposed for accurate prediction of HEMT performance [14-19] but there is room for improvement in the model through properly addressing the above issues related to advanced HEMT structures.

Hot electron conditions are developed in a QW if the applied electric field is sufficiently high (in the present case it is around 10^6 V/m) so as to cause a pronounced derivation from Ohm's low [20]. At these fields the drift energy of the carriers may be compared to the thermal energy and the symmetric term is no longer the equilibrium distribution at the lattice temperature [21-22]. In the presence of an electric field parallel to the heterojunction interfaces, the carrier distribution function is heated drifted Fermi-Dirac distribution for the carriers characterized by an electron temperature T_e, and a drifted crystal momentum p_d [21-24]. The establishment of an electron temperature is evident from the photoluminescent experiments [25-26]. Some mobility models incorporating the effects of hot electrons and relevant scattering mechanisms have already been proposed and developed for QW structures [21-23]. This model is generally known as hydrodynamic model which is accurate but not suitable to be incorporated in the TCAD circuit simulator due to it's time consuming and numeric type of nature. On the other hand drift-diffusion model is less accurate but suitable to be incorporated in the circuit simulator due to it's less time consumption and analytic type of nature. Same time it is difficult to incorporate different

short channel phenomenon in drift diffusion model accurately, especially in HEMT modeling. So, in the present case we have adopted a mixed mode approach for HEMT modeling. First, we have derived a hydrodynamic mobility model based on energy and momentum balance equations but our approach and assumptions are formulated in such a way that the mobility model is fast converging and it's nature is analytic. Then the mobility model has incorporated in drift diffusion model to develop a QW HEMT analytical model. Different elastic and non elastic scattering mechanisms are considered to calculate overall energy and momentum loss rate. Present analytical model has used to study the electron transport phenomena through current voltage and conductance analysis. Although the proposed model is applicable for other HEMT structures, $Al_xGa_{1-x}As/GaAs$ HEMT structure is considered in this work to simulate some results for comparison with experimental results to validate its accuracy.

2. Theory

The cross-sectional geometry and energy profile of a quantum well HEMT model is shown in figure 1.

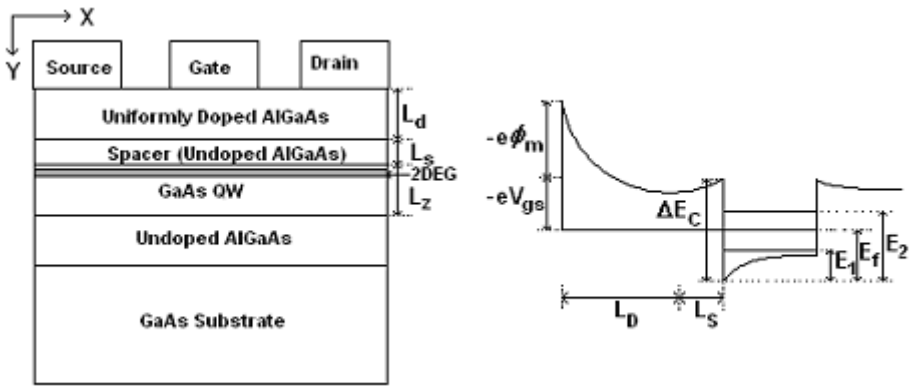

Fig. 1: Cross-sectional geometry and energy profile of quantum well HEMT model.

The carrier concentration at any point in the conducting channel is modeled as a function of gate to source voltage and channel potential. Current density at any point of the channel is a function of carrier concentration, electron mobility and field at that point. The conducting channel is formed by an undoped GaAs layer of thickness L_Z, sandwiched between two $Al_xGa_{1-x}As$ barrier layers. Carriers in the channel are supplied by the homogeneously doped $Al_xGa_{1-x}As$ layer located at L_S from the well.

2.1 n_s-V_{gs} Model

The relationship between the two dimensional electron gas (2DEG) or sheet carrier concentration (n_s) and the applied gate voltage (V_{gs}) in the quantum well using the charge control model is given by [2];

$$n_S = \frac{\varepsilon_1}{e\left(L_D + L_S + \Delta L\right)}\left(V_{gs} - V_{th}\right) \tag{1}$$

Where L_D is the donor layer thickness, L_S is the spacer layer thickness, ΔL (≈8 Å) is a curve-fitting parameter representing the effective thickness of the 2DEG, and V_{th} is the threshold voltage. The threshold voltage is given by;

$$V_{th} = \phi_m - \Delta E_C - \frac{eN_d}{2\varepsilon_1} L_D{}^2 + \Delta E_{FO} (2)$$

Here, ϕ_m is the Schottky barrier height, ΔE_C is the conduction band discontinuity, N_d is the doping concentration of the doped layer, ε_1 is the permittivity of and ΔE_{FO} is another curve-fitting parameter equal to 0 and 25mV at 300K and 77K respectively [3,4]. In the presence of a drain bias n_s is given as;

$$n_S = \frac{\varepsilon_{AlGaAs}}{e(L_D + L_S + \Delta L)} \left(V_{gs} - V_{th} - V(x)\right) \quad (3)$$

where *V(x)* is the channel potential. To include sub-threshold, moderate and strong inversion region, eqn. (3) is modified as;

$$n_S(x) = \frac{\varepsilon_{AlGaAs}}{e(L_d + L_S + \Delta L)} \left\{1 + A\exp\left(-B\left(V_{gs} - V_{th} - V(x)\right)\right)\right\}^{-1} \quad (4)$$

The coefficients *A* and *B* are used to fit eqn. (4) to the charge resulting from an exact numerical solution. Considering strong inversion we have used eqn.3 for further analysis with less complexity.

2.2 Mobility Model

Improved carrier concentration and reduced ionized impurity scattering in the QW-HEMT establish a strong electron-electron interaction, favouring a heated drifted Fermi-Dirac distribution function for the carriers characterized by an electron temperature T_e, and a drifted crystal momentum p_d [20-23]. In the presence of an electric field applied parallel to the hetero junction interface, the carrier distribution function $f\left(\vec{k}_{\|}\right)$ can be expressed as;

$$f\left(\vec{k}_{\|}\right) = f_0(E) + \frac{\hbar |\overrightarrow{p_d}||\overrightarrow{k_{\|}}|}{m^*}\left(-\frac{\partial f_0}{\partial E}\right)\cos\gamma \quad (5)$$

where, *fo(E)* is the Fermi-Dirac distribution function for the carriers, $\vec{p}_d$ is the drift crystal momentum, $\hbar$ is Planck's constant divided by 2π, $\vec{k}_{\|}$ is the two-dimensional wave vector of the carriers with energy *E*, m* is the electronic effective mass and γ is the angle between the applied electric field and the two dimensional wave vector $\vec{k}_{\|}$.

The energy and momentum balance equations obeyed by the carrier are;

$$ep_d F / m^* + \langle dE/dt \rangle_{scat} = \frac{d\langle E \rangle}{dt} \tag{6}$$

and

$$eF + \langle dp_d / dt \rangle_{scat} = \frac{dp_d}{dt} \tag{7}$$

Where $\langle dp_d / dt \rangle_{scat}$ and $\langle dE/dt \rangle_{scat}$, represents, respectively, the average momentum and energy loss rates due to scatterings and $\langle E \rangle$ depicts the average energy of a carrier with charge e. Knowing the value of n_s and T_e at every point along the channel, dc mobility can be calculated throughout the channel using the following two equations (detailed derivation shown in Appendix):

$$\mu_{dc}(x) = \frac{b_3 + b_1 T_e(x) + b_2 n_S(x)}{m^* F_0 + m^* F(x)} \qquad for \qquad F < F_C \tag{8}$$

and

$$\mu_{dc}^{sat} = \frac{p_d(T_e^c, n_S^{\min})}{m^* F_C} \qquad for \quad F \geq F_C \tag{9}$$

2.3 Current Voltage Model

From the current density equation [27], the drain current is given as;

$$I_{ds}(x) = we\mu_{dc}(x)\left(n_s(x)\frac{dV(x)}{dx} + \frac{k_B T}{e}\frac{dn_s(x)}{dx} \right) \tag{10}$$

Applying the boundary conditions $V(0) = I_{ds} R_S$ at x=0 and $V(L_C) = V_{ds} - I_{ds}(R_S + R_d)$ at x=L_C, the drain current in the linear region is derived as;

$$I_{ds}^2[a_1 + m^*(R_S + R_D)] - I_{ds}[wea_2(R_S + R_D) + 2a_3(R_S + R_D)V_{DS} - m^* V_{DS} - m^* F_0 L_C] + a_3 V_{ds}^2 + wea_2 V_{ds} = 0 \tag{11}$$

Here, $a_3 = \frac{\varepsilon_{AlGaAs}}{e^2 L_T^2}\{b_2(V_{gs}^{eff} - V_{th}) - \frac{b_4}{2}\}$, $a_2 = \frac{\varepsilon_{AlGaAs}}{eL_T}(V_{gs}^{eff} - V_{th})\{b_4 + \frac{b_2 \varepsilon_{AlGaAs}}{eL_T}(V_{gs}^{eff} - V_{th})\}$, $a_1 = a_3(2R_S^2 + 2R_S R_D + R_D^2)$ $L_T = L_d + L_S + \Delta L$, $V_{gs}^{eff} = V_{gs} - I_{ds} R_S$, w is channel width, L_C is channel length, R_S and R_D are the source and drain resistance, respectively. Taking the derivative of I_{ds} with respect to V_{ds} and equating it to zero, the saturation drain current I_{dsat} is obtained as;

$$I_{ds,sat} = \frac{wea_2 + 2a_3 V_{dast}}{2a_3(R_S + R_D) - m^*} \tag{12}$$

Considering velocity saturation and recalculating eqn. 10 with eqn. 9, the expression for the saturation current can be calculated from

$$I_{ds,sat}^2[m^*(2R_S+R_D)-\frac{a_4\varepsilon_{AlGaAs}}{2eL_T}(2R_S^2+2R_SR_D+R_D^2)]$$

$$+I_{ds,sat}[\frac{a_4\varepsilon_{AlGaAs}}{eL_T}(R_S+R_D)V_{dsat}-(2R_S+R_D)a_4a_5-m^*F_CL_C-m^*V_{dsat}] \quad (13)$$

$$+a_4a_5V_{dsat}-\frac{a_4\varepsilon_{AlGaAs}}{2eL_T}V_{ds}^2=0$$

Here, $a_4=wep_d(T_L,n_{2D}^{\min})$, $a_5=\frac{\varepsilon_{AlGaAs}}{eL_T}[(V_{gs}^{eff}-V_{th})-\frac{k_BT_L}{e}]$

Now equating the value of $I_{ds,sat}$ from equation 12 and 13 we obtained

$$V_{dsat}^2(a_8a_7^2-\frac{a_4\varepsilon_{AlGaAs}}{2eL_T}-a_9a_7)+V_{dsat}(a_6a_9-a_7a_{10}+a_4a_5+2a_6a_7a_8)-a_7a_{10}+a_6^2a_8=0$$

(14)

Here, $a_6=\frac{wea_2}{2a_3(R_S+R_D)-m^*}$, $a_7=\frac{2a_3}{2a_3(R_S+R_D)-m^*}$,

$a_8=[m^*(2R_S+R_D)-\frac{a_4\varepsilon_{AlGaAs}}{2eL_T}(2R_S^2+2R_SR_D+R_D^2)]$, $a_9=\frac{a_4\varepsilon_{AlGaAs}}{eL_T}(R_S+R_D)-m^*$ and

$a_{10}=(2R_S+R_D)a_4a_5-m^*F_CL_C$.

Trans-conductance calculated for linear and saturation regions are given as;

$$g_{m,lin}=\frac{I_{ds,lin}[we(R_S+R_D)a_{11}+2V_{ds}(R_S+R_D)a_{12}]}{we(R_S+R_D)a_2+2V_{ds}(R_S+R_D)a_3} \quad (15)$$

and

$$g_{m,sat}=\frac{wea_{11}+2a_{12}V_{dsat}}{2a_3(R_S+R_D)-m^*} \quad (16)$$

Here, $a_{11}=\frac{\varepsilon_{AlGaAs}}{eL_T}[b_4+\frac{2b_2\varepsilon_{AlGaAs}}{eL_T}(V_{gs}^{eff}-V_{th})]$ and $a_{12}=\frac{b_2\varepsilon_{AlGaAs}^2}{e^2L_T^2}$.

In the present analysis, we have considered $I_{ds}R_S\langle\langle V_{gs}$ and under this consideration $V_{gs}^{eff}=V_{gs}$. This consideration is proposed to avoid the formation of third order drain current equation and related complexity.

3. Results and Discussion

Numerical results are simulated for $Al_xGa_{1-x}As$/GaAs QW-HEMT structure using the parameters given in Table 1. To confirm the validity of the proposed analytical model simulated results are compared with available experimental results [28, 29].

Table 1: Parameters used for simulation.

Parameters	Value
HEMT Model	
AlGaAs, doping Conc. (m^{-3})	2×10^{18}
Φ_m	1.0 eV
L_S	3nm
ΔL	0.5nm
L_d	30nm
ε_{AlGaAs}	1.07×10^{-12}
ΔE_C	0.286eV
w	100μm
L_C	1μm
v_{sat}	1.8×10^5 m/sec
F_C	350 KV/m
$R_S=R_D$	5.4 Ω
Mobility Model (SI unit)	
Electron Effective Mass	0.61033×10^{-31}
Longitudinal Elastic Constant(Nm^{-2})	14.03×10^{10}
Acoustic Deformation Potential	17.6×10^{-19}
Static Dielectric Constant	12.53
Optic Dielectric Constant	10.82
LO Phonon Angular Frequency	5.37×10^{13}

The variation of sheet carrier concentration with gate voltage can be divided into three regions: the sub-threshold region, the linear region and the saturation region. The linear region corresponds to direct modulation of n_s by the gate bias. The doped layer is almost completely ionized in the linear region. In the saturation region, the doped layer is partially ionized. Electric flux changes are shielded by this layer and the gate can no longer modulate 2DEG carrier concentration. Representing the three regions with a single equation needs some careful fitting parameters. Variation of sheet carrier or 2-D electron concentration is plotted using equation 4 (fitted with A=0.5, B=7) and results are shown in the fig. 2. The results are in good agreement with the experimental results presented in Ref. 28.

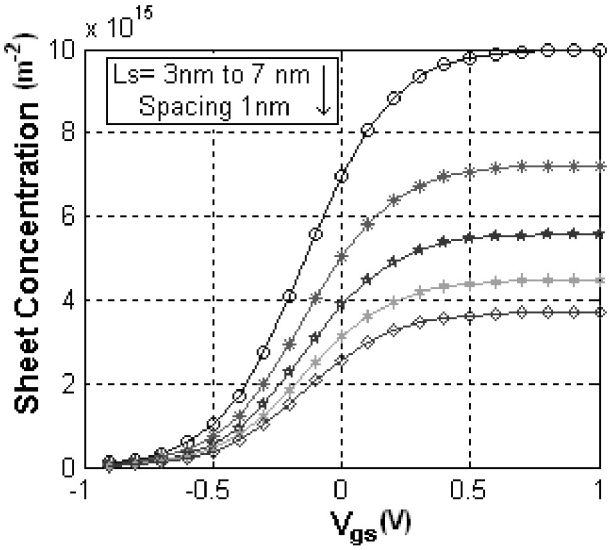

Fig. 2: Variation of two dimensional electron gas (2DEG) concentrations with effective gate voltage

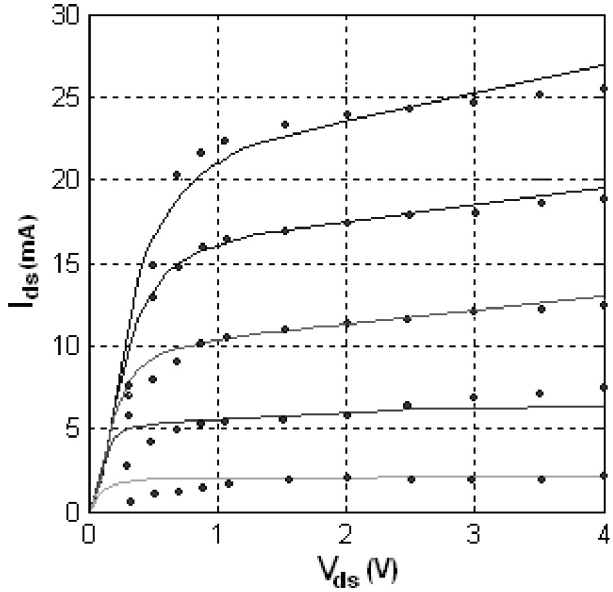

Fig. 3: I-V characteristics for gate voltage range Vgs: -0.3 to 0.5 V with 0.2 V steps. Solid curves: our model, dots: experimental data.

Figure 3 shows the variation of drain current with drain voltage for different applied gate voltages. It is clear from the figure that the experimental results [28,29] and the outcome of the analytical model are in good agreement. The variation of drain current with gate voltage for different values of drain voltage is shown in figure 4. After a certain gate voltage, sheet concentration starts to saturate and the effect of saturation is reflected on drain current [30]. At low voltage hot electron condition may be relaxed which causes some deviation of simulated results from the experimental values.

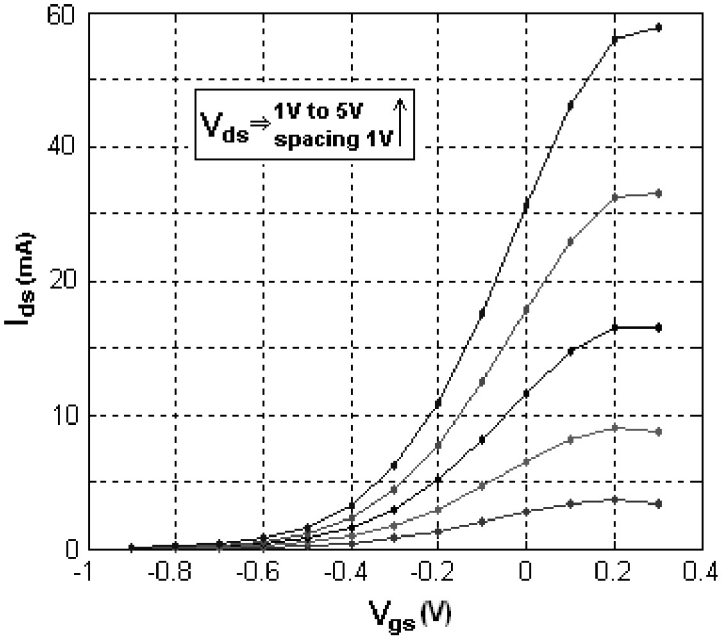

Fig. 4: Variation of drain current with effective gate voltage for different drain bias.

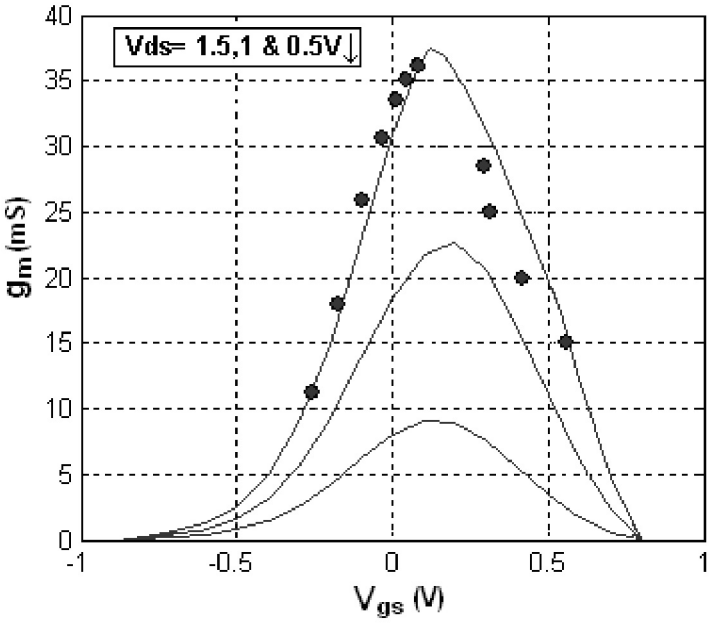

Fig. 5: Variation of transconductance with gate voltage for different drain bias. Solid line: our model, Dots: Experimental data.

The variation of trans-conductance with gate voltage is computed and compared with the experimental results [28, 29] to substantiate the validity of our model and results are shown in the figure 5. Our analytical model accurately predicted the value of maximum trans-conductance.

4. Conclusion

A field dependent mobility model, incorporating the variation of sheet carrier concentration and electron temperature along the channel is developed. Our model successfully predicted the electron mobility at every position along the channel under certain assumptions. Some short channel phenomena have not been included in the present analysis for simplicity but can be incorporated for enhancing the accuracy of advanced short channel HEMT structure modeling. Our mobility model has been used in the Drift-diffusion carrier transport model to calculate the drain current. The sheet carrier concentration, *I-V* characteristics and conductance of $Al_xGa_{1-x}As/GaAs$ QW-HEMT structure are calculated. The results obtained from our model are found to be in good agreement with experimental results thereby establishing the validity of the proposed model. This analysis is very useful for analytical model development of advanced short channel QW-HEMT structure as new and unavoidable physical phenomena comes into picture with reduced device dimensionality.

Acknowledgement

Sanjoy Deb thankfully acknowledges the financial support obtained from School of Material Science and Nanotechnology, Jadavpur University in the form of UGC Fellowship.

Appendix*: *Derivation of field dependent mobility μ_{dc}^{lin} *and* μ_{dc}^{sat}

The energy and momentum relaxation time for different scattering mechanisms are calculated. The mobility model is then derived using the energy and momentum balance equations. The scattering rate calculation for different scattering mechanisms is given in section *A*. The energy and momentum balance equations are given in sections *B* and *C*, respectively. Finally, the calculation of mobility is given in section *D*.

A: Scattering Rate Calculation

It is assumed that the quantum well width and carrier concentration is not sufficiently high so that inter-sub-band scattering can be neglected [20]. The channel length is considered not too short and field not too high for generation of velocity overshoot and ballistic transport effect. These affects can be incorporated in the present mobility model with modification of scattering rate but deliberately avoided in the present model to reduce complexity.

A.1: LO Phonon Scattering Rate

Generalized scattering rate for LO phonon is given by [25];

$$\frac{1}{\tau_{lo}} = \frac{|c|^2 v}{4\pi^2\hbar}\left(N_q + \frac{1}{2} \pm \frac{1}{2}\right)\int d\phi \int q_{\|} dq_{\|} I_{2D}\left(q_{\|}, L_Z\right)\delta\left[E' - E \pm \hbar\omega\right] \qquad \text{(A.1)}$$

Where, $|c|^2 = \frac{2\pi}{v} e^2\hbar\omega\left(\frac{1}{\varepsilon_\infty} - \frac{1}{\varepsilon_s}\right)$, Final state electron energy $E' = E\left(\vec{k}_{\|} \mp \vec{q}_{\|}\right), q_{\|}$ is the phonon parallel wave vector , N_Q is phonon occupation number, ε_s and ε_∞ are the static and high frequency dielectric constant, $\hbar$ is the Planck's constant divided by 2π, ω is the LO phonon angular frequency.

Scattering rate for LO phonon absorption process is given by;

$$\frac{1}{\tau_a} = \frac{\alpha\omega}{\pi} N_q \int_0^{\pi} d\phi \frac{q_+^a(E,\phi) I_{2D}\left[q_+^a(E,\phi), L_Z\right]}{\sqrt{\frac{E}{\hbar\omega}\cos^2\phi + 1}} \tag{A.2}$$

Scattering rate for LO emission process is given by;

$$\frac{1}{\tau_e} = \frac{\alpha\omega}{\pi}\left(N_q + 1\right) \int_0^{\phi_{\max}} d\phi \frac{q_+^e(E,\phi) I_{2D}\left[q_+^e(E,\phi), L_Z\right] + q_-^e(E,\phi) I_{2D}\left[q_-^e(E,\phi), L_Z\right]}{\sqrt{\frac{E}{\hbar\omega}\cos^2\phi - 1}} \tag{A.3}$$

Where $\alpha = \frac{1}{2}\frac{e^2}{\sqrt{\hbar/2m^*\omega}}\left(\frac{1}{\varepsilon_\infty} - \frac{1}{\varepsilon_s}\right)\Big/\hbar\omega$ (A.4)

A.2: Acoustic Phonon Scattering Rate

Expression of acoustic phonon scattering rate is given as [31];

$$\frac{1}{\tau_{ac}} = \frac{3\left(m^*\right)^{1.5} E_1^2 T_1}{4\sqrt{2}\pi^2\hbar^4 C_1 L n_S e T_e} \frac{1}{\beta^2 E} \int_0^{2\beta\sqrt{E}} \frac{(q^{ac})^2 S^2\left(q^{ac}\right)}{\sqrt{1 - \frac{(q^{ac})^2}{4\beta^2 E}}} dq^{ac} \tag{A.5}$$

Here $\beta = \frac{\sqrt{2m^*}}{\hbar}$ and $S(q^{ac})$ is the two dimensional screening potential and is given as;

$$S\left((q^{ac})\right) = \frac{(q^{ac})}{(q^{ac}) + \chi H\left((q^{ac})\right)}$$

Here $\chi = \frac{e^2 m^*}{2\pi\varepsilon_0\varepsilon_S\hbar^2}$ and

$$H\left((q^{ac})\right) = \left\{\frac{4}{\left(4\pi^2 + L_Z^2(q^{ac})^2\right)}\right\}\left[\frac{3}{4}L_Z q^{ac} + \frac{2\pi^2}{L_Z q^{ac}} - \frac{8\pi^4\left(1 - \exp\left(-L_Z q^{ac}\right)\right)}{L_Z^2(q^{ac})^2\left(4\pi^2 + L_Z^2(q^{ac})^2\right)}\right]$$

Here q^{ac} is the scattering vector, E_1 is the acoustic deformation potential and C_1 is the longitudinal sound velocity.

A.3: Ionized Impurity Scattering Rate

Remote ionized impurity scattering is ignored in the present case and background ionized impurity scattering rate is given as [32];

$$\frac{1}{\tau_{im}} = \frac{\pi^3 m^* L_Z^3 N_i e^4}{\varepsilon_0^2 \varepsilon_S^2 \hbar^3} \int_0^{\pi/2} \left[\frac{6x^6}{\rho^2 \pi^4} + \frac{8x^4}{\rho^2 \pi^2} - \frac{x}{2\rho^2} \left(\exp(-4x) + 4(1-\exp(-2x)) \left(1 + \frac{x}{2} + \frac{x^2}{x^2+\pi^2} \right) - 1 \right) \right] \quad \text{(A.6)}$$
$$\left[4x^4 + x^2 \left(4\pi^2 + 3\vartheta \right) + 2\pi^2 \vartheta \right]^{-2} d\theta$$

Here $\rho = k_{\|} L_Z$, $x = \rho \cos\theta$, $\vartheta = \frac{e^2 m^* L_Z}{2\pi\hbar^2 \varepsilon_0 \varepsilon_S}$, θ is the scattering angle and N_i is the background ionized impurity concentration.

B: Energy Balance Equation

Energy balance equation of the carrier is given by;

$$ep_d F / m^* + \langle dE/dt \rangle_{scat} = \frac{d\langle E \rangle}{dt} \quad \text{(A.6)}$$

Energy balance equation is solved for non elastic scattering (LO Phonon scattering) and for a degenerate system the solution will be [21-24];

$$Fp_d = g_1(T_e, n_S)$$
(A.7)

Here,

$$g_1 = \frac{(m^*)^2 e\omega(\varepsilon_S - \varepsilon_\infty)}{8\pi^2 \hbar^2 n_S \varepsilon_0 \varepsilon_S \varepsilon_\infty \sqrt{\hbar/(2m^*\omega)}} \left((N_Q + 1) \int_{\hbar\omega}^{\infty} I_{2D}^1(E, T_e) f_0(E)[1 - f_0(E - \hbar\omega)] dE \right. \quad \text{(A.8)}$$
$$\left. - N_Q \int_0^{\infty} I_{2D}^2(E, T_e) f_0(E)[1 - f_0(E + \hbar\omega)] dE \right)$$

and in the expression of g_1,

$$I_{2D}^1 = \int_0^{\pi} q_+^a(E,\phi) I_{2D}\left[q_+^a(E,\phi), L_Z \right] \left[\sqrt{\left(\frac{E}{\hbar\omega} \right) \cos^2\phi + 1} \right]^{-1} d\phi$$

$$I_{2D}^2 = \int_0^{\phi_{\max}} \left\{ q_+^e(E,\phi) I_{2D}\left[q_+^e(E,\phi), L_Z \right] + q_-^e(E,\phi) I_{2D}\left[q_-^e(E,\phi), L_Z \right] \right\} \left[\sqrt{\left(\frac{E}{\hbar\omega} \right) \cos^2\phi - 1} \right]^{-1} d\phi$$

C: Momentum balance equation

Momentum balance equation is given by;

$$eF(x) + \langle dp_d / dt \rangle_{scat} = \frac{dp_d}{dt} \quad \text{(A.9)}$$

The solution of the momentum balance equation for all elastic and non elastic scattering mechanisms is given as [21-24];

$$\frac{F}{p_d} = e^{-1}T_e^{-1}\left\langle \frac{dp_d}{dt} \right\rangle_{scat} = g_2(T_e, n_S) \tag{A.10}$$

Here $\left\langle \frac{dp_d}{dt} \right\rangle_{scat}$ is the average momentum loss rate for the all scattering mechanism and this is given as;

$$\left\langle \frac{dp_d}{dt} \right\rangle_{scat} = \left\langle \frac{dp_d}{dt} \right\rangle_{LO} + \left\langle \frac{dp_d}{dt} \right\rangle_{ac} + \left\langle \frac{dp_d}{dt} \right\rangle_{im} \tag{A.11}$$

Individual average momentum loss rate for different scattering mechanisms are given as;

LO phonon;

$$\left\langle \frac{dp_d}{dt} \right\rangle_{LO} = y_1\left((N_Q+1)\int_{\hbar\omega}^{\infty} I_{2D}^3(E) f_0(E)[1-f_0(E)][1-f_0(E-\hbar\omega)]E^{1/2}dE \right.$$
$$\left. - N_Q\int_0^{\infty} I_{2D}^4(E) f_0(E)[1-f_0(E)][1-f_0(E+\hbar\omega)]E^{1/2}dE \right) \tag{A.12}$$

Here, $y_1 = \dfrac{e^2(\varepsilon_S - \varepsilon_\infty)(m^*)^{0.5}}{8\sqrt{2}\pi^3\hbar^2\varepsilon_0\varepsilon_S\varepsilon_\infty n_S k_B T_e\sqrt{\hbar/(2m^*\omega)}}$,

$$I_{2D}^3 = \int_0^{\pi}\left[q_+^a(E,\phi)\right]^2 I_{2D}\left[q_+^a(E,\phi), L_Z\right]\left[\sqrt{\left(\frac{E}{\hbar\omega}\right)\cos^2\phi + 1}\right]^{-1}\cos\phi\, d\phi \quad \text{and}$$

$$I_{2D}^4 = \int_0^{\phi_{\max}}\left[\left[q_+^e(E,\phi)\right]^2 I_{2D}\left[q_+^e(E,\phi), L_Z\right] + \left[q_-^e(E,\phi)\right]^2 I_{2D}\left[q_-^e(E,\phi), L_Z\right]\right].....$$
$$.....\left[\sqrt{\left(\frac{E}{\hbar\omega}\right)\cos^2\phi - 1}\right]^{-1}\cos\phi \quad d\phi$$

Acoustic phonon;

$$\left\langle \frac{dp_d}{dt} \right\rangle_{ac} = \frac{3(m^*)^{3/2}E_1^2T_L}{4\sqrt{2}\pi^2\hbar^4C_1Ln_ST_e}\int_0^{\infty}\frac{1}{\beta^2E}\int_0^{2\beta\sqrt{E}}\frac{(q^{ac})^2S^2(q^{ac})}{\sqrt{1-\dfrac{(q^{ac})^2}{4\beta^2E}}}dq^{ac}f_0(E)[1-f_0(E)]E^{1/2}dE \tag{A.13}$$

Ionized Impurity;

$$\left\langle \frac{dp_d}{dt} \right\rangle_{im} = \frac{\pi^2(m^*)^2L_Z^3N_ie^3}{\varepsilon_0^2\varepsilon_S^2n_Sk_B\hbar^5T_e}\int_0^{\infty}\gamma(E)f_0[1-f_0(E)]EdE \tag{A.14}$$

$$\gamma(E)=\int_0^{\pi/2}\frac{x}{K^2}\left[\frac{6x^5}{\pi^4}+\frac{8x^3}{\pi^2}+0.5\left(1-\exp(-4x)-4(1-\exp(-2x))\left(1+\frac{x}{2}+\frac{x^2}{x^2+\pi^2}\right)\right)\right]$$
$$\left[4x^4+x^2\left(4\pi^2+3p\right)+2\pi^2 p\right]^{-2}d\theta$$

Here, $f_0(E)$ is the Fermi-Dirac distribution function at electron temperature T_e and sheet carrier concentration n_S. Significances of other symbols used for mobility calculation are given in Ref [21-24].

D: Mobility Calculation

For a fixed value of other parameters and known value of T_e and n_s, we can calculate $g_1(T_e,n_s)$, $g_2(T_e,n_s)$. Using equations A.7 and A.10 and representing them as a function of n_S and T_e, we can write;

$$p_d(T_e,n_S)=\sqrt{\frac{g_1(T_e,n_S)}{g_2(T_e,n_S)}} \tag{A.15}$$

From $p_d(T_e,n_s)$, mobility can be calculated using velocity-mobility-field relation;

$$\mu_{dc}=\frac{p_d(T_e,n_S)}{m^*F} \tag{A.16}$$

Here $F=F_0+F(x)$ is the total field which consists of a low value component F_0 due to the potential at the channel terminal at the source end (x=0) [33] and a variable component $F(x)$ given as $\left(\frac{dV(x)}{dx}\right)$ due to the applied voltage between source and drain terminal.

From A.15 and A.16 we can write;

$$F=\sqrt{g_1(T_e,n_S)g_2(T_e,n_S)} \tag{A.17}$$

This approach gives 2-D mobility as function of x and y but T_e, n_S and F are considered only as functions of x so this will effectively reduce $\mu(x,y)$, independent of y.

Now as we considered both T_e and n_s varies with x, we have to present both the factors as x dependent functions. For doing so, some simple assumptions are considered which are given as follows;

i. Electron is at lattice temperature (T_e=T_L) and $n_S=n_S^{\max}$, at the channel-source terminal and $n_S^{\max}$ (maximum sheet carrier concentration, at x=0) can be computed with eqn.3, considering channel potential is zero. With T_e=T_L and $n_S=n_S^{\max}$, F_0 can be calculated with eqn. A.17.

ii. Along the channel electron temperature will increase and sheet carrier concentration will decrease and at the saturation point channel will pinch off along with electron velocity saturation.

iii. The saturation point is very close to drain and at that point $n_S = n_S^{\min}$ and $n_S^{\min}$ (minimum sheet carrier concentration at x=L_C) can be estimated with eqn.3, considering channel potential is equal to drain bias.

iv. At the point of saturation electron temperature is defined as critical electron temperature (T_e^c) and this variation from T_L to T_e^c is considered to be linear along the channel. For a considered value a critical electric field and computed value of $n_S^{\min}$, critical electron temperature can be estimated from equation A.17.

v. At the point of saturation, $F=F_C, n_S = n_S^{\min}$ and $T_e = T_e^c$.

vi. Beyond the saturation point, electron temperature saturates at critical electron temperature (T_e^c) and sheet carrier concentration to its minim value ($n_S^{\min}$).

Now from eqn. A.16, mobility equation in the linear region can be written as;

$$\mu_{dc}^{lin} = \frac{p_d(T_e(x), n_S(x))}{m^* F_0 + m^* F(x)} \qquad for \quad F < F_C \tag{A.18}$$

Considering the boundary conditions on $T_e(x)$ and $n_S(x)$ and using taylor series expansion and eliminating the higher order terms the above equation can be rewritten as;

$$\mu_{dc}^{lin} = \frac{p_d(T_L, n_S^{\max}) + (T_e - T_L)\frac{dp_d(T_L, n_S^{\max})}{dT_e} + (n_S - n_S^{\max})\frac{dp_d(T_L, n_S^{\max})}{dn_S}}{m^* F_0 + m^* F(x)} \tag{A.19}$$

Farther simplification, the expression can be written as;

$$\mu_{dc}^{lin} = \frac{b_3 + b_1 T_e(x) + b_2 n_S(x)}{m^* F_0 + m^* F(x)} \qquad for \qquad F < F_C \tag{A.20}$$

Here, $b_1 = \frac{dp_d(T_L, n_S^{\max})}{dT_e}, b_2 = \frac{dp_d(T_L, n_S^{\max})}{dn_{2D}}$ and $b_3 = p_d(T_L, n_S^{\max}) - T_L b_1 - n_S^{\max} b_2$.

Mobility beyond the saturation point is expressed as;

$$\mu_{dc}^{sat} = \frac{p_d(T_e^c, n_S^{\min})}{m^* F_C} \qquad for \quad F \geq F_C \tag{A.21}$$

Mobility expressions given in A.20 and A.21 are used to calculate currents at linear and saturation regions, respectively.

References

[1] T. Mimura, S. Hiyamizu, T. Fujii, K. Nanbu, Japan J. Appl. Phys., **19** (1980) 225
[2] D. Delagebeaudeuf, T, N, Linh, IEEE Trans. Electron Devices, **29** (1982) *955*
[3] K. Lee, S. M. Shur, J. T. Drummond, G. H. Morko, IEEE Trans. Electron Devies, **30** (1983) 207
[4] V. Guru, J. Jogi, M. Gupta, H. P. Vyas, S. R. Gupta., Microwave. Optical Technology Lett., **37** (2003) 376
[5] K. Lee, S. M. Shur, J. T. Drummond, G. H. Morko, J. Appl. Phys., **54** (1983) 2093.
[6] K. Lee, S. M. Shur, J. T. Drummond, G. H. Morko, IEEE Trans. Electron Devies, **31** (1984) 29
[7] G. Meneghesso, F. Zanon , M. Uren, E. Zanoni, IEEE Electron Devices Lett., **30** (2009) 100
[8] Y. Pei, Z. Chen, D. Brown, S. Keller, S. P. Denbaars, U. Mishra, IEEE Electron Devices Lett*.,* **30** (2009) 328
[9] F. Ali, A. Gupta. *HEMTs and HBTs: Devices, Fabrication and Circuits*, Editors, Artech House, Boston, (1991)
[10] S. Adachi, *Properties of Group-IV, III–V and II–VI Semiconductors***,** John Wiley & Sons Ltd, West Sussex, England (2005)
[11] M. Passlack, J. K. Abrokwah, R. Lucero, IEEE Electron Devices Lett., **21** (3) (2000) 518
[12] Kevin F. Brennan, April S. Brown, *Theory of Modern Electronic Semiconductor Devices*, John Wiley & Sons, Inc., New York. (2002)
[13] N. Goela, S. J. Chunga, M. B. Santosa, K. Suzukib, S. Miyashitab, Y. Hirayamab, *Ballistic transport in InSb mesoscopic structures*, Physica E **21** (2004) 761
[14] P. K. Jaydeep, K. Roy, IEEE Trans. Electron Devices **55** (2008) 2537
[15] S. Vitanov, V. Palankovski, S. Murad, T. Rodle R. Quay, S. Selberherr, Simulation of semiconductor process and devices **12** (2007) 273.
[16] P. Roblin, S. C. Kang, H. Morkoc, **37** (1990) 1608.
[17] A. Mehmet, O. Turkoglu, Physica B **348** (2004) 272.
[18] A. Rashmi, A Kranti, S. Haldar, S. R. Gupta, Solid-State Electronics, **46** (2002) 621
[19] K. Kalna, S. Roy, A. Asenov, K. Elgaid, I. Thayne, Solid-State Electronics, **46** (2002) 631
[20] D. Chattopadhyay, Phys. Rev. B. **33** (1986) 7288
[21] S. K. Sarkar, D. Chattopadhyay, Nanotechnology **2 (1)** (1998)321
[22] S. K. Sarkar P. K. Ghosh D. Chattopadhyay, J. Appl. Phys. **78** (1995) 283
[23] D. Chattopadhyay, Appl. Phys. A, 53 (1991) 35.
[24] Sanjoy Deb, N. Basanta Singh, Subir Kumar Sarkar, Physica B, **404** (2009) 3727
[25] J. P. Leburton, *J. Appl. Phys.,* **56** (1984) 2850
[26] J. M Carson, S. A. Lyon, J. M. Worlock, A.c. Gossard, W. Wiegmann, Bull. Amer. Phys. Soc. **29** (1984) 213
[27] K. R. Tyagi, A. Ahlawat, M. Pandey, S Pandey, Microelectronics Journal, **38** (2007) 877
[28] M. A. Aziz, M. El-Sayed, M. El-Banna, Solid-State Electronics, **43** (1999) 891
[29] R. H. Yeager, W. R. Dutton, IEEE Transactions on Electron Device, **33** 5 (1986) 682
[30] I. Thayne, K Elgaid, D. Moran, X. Cao, E. Boyd, H. McLelland, M. Holland, S Thoms, C. Stanley, Thin Solid Films, **515** (2007) 4373
[31] D. Chottopadhyay, Physics Status Solidi B, **135** (1986) 409
[32] J. Lee, H. N. Spector, V. K. Arora, J. Appl. Phys. **54** (1983) 6995
[33] R. Sing, M. C. Snowden, IEEE Transactions on Electron Device, **45**(1998)1165